Separation Science and Technology, 41: 1001–1023, 2006

ISSN 0149-6395 print/1520-5754 online
DOI: 10.1080/01496390600641611

Taylor & Francis
Taylor & Francis Group

Centrifugal Contactors: Separation of an Aqueous and an Organic Stream in the Rotor Zone (LA-UR-05-7800)

Nely T. Padial-Collins, Duan Z. Zhang, Qisu Zou, and Xia Ma
Computer and Computational Sciences Division Group CCS-2,
Continuum Dynamics, Los Alamos, New Mexico, USA

W. Brian VanderHeyden
Nonproliferation & Security Technology Program Office (N-NST),
Washington, DC, USA

Abstract: A multi-phase flow code is used to simulate the separation of an aqueous and an organic stream in the rotor zone of an annular centrifugal contactor. Different values for the mixture viscosity and for the initial volume fractions of the components are considered. A simple model for mass transfer of a species between phases is used. Geometrical effects are found to have significant influence on the separation of the two-phase mixture.'

Keywords: Separation, multi-phase flow, mixture viscosity, mass transfer, numerical simulation

INTRODUCTION

The development of annular centrifugal contactors began at the National Laboratories more than three decades ago. The first centrifugal contactors were devised at the Savannah River Laboratory (SRL) and, subsequently

Received 18 October 2005, Accepted 7 February 2006
This work was carried out under the auspices of the National Nuclear Security Administration of the U.S. Department of Energy at Los Alamos National Laboratory under Contract No. W-7405-ENG-36.
Address correspondence to Nely T. Padial-Collins, Computer and Computational Sciences Division Group CCS-2, Continuum Dynamics, MS D413, Los Alamos, New Mexico, 87544, USA. E-mail: nelylanl@lanl.gov

modified at Argonne National Laboratory (ANL) to the form known as the annular centrifugal contactor. A reasonably complete description of the technology has been provided in papers by ANL scientists (1–4). The contactors consist of a vertical centrifuge providing for both the mixing and for the separating of liquids in a single unit. They can be easily interconnected to allow multistage processing. In each contactor, two immiscible liquids are fed into the annulus, formed by the spinning rotor and the stationary housing wall, through different inlets close to the top of the device. The liquids mixed in the annular region are pumped into the rotor bottom. Upon entering the rotor region or separation zone, the liquids are accelerated to the wall with the heavier fluid going to the outside. Each liquid leaves the device through an exit port. Transfer of a species between the two phases depends on the extent of the contacting surface, on the separation between the two phases, and the time of contact between the phases.

A large part of the prediction and analysis of the results of centrifugal contactor experiments has been made, chiefly, through flow sheet simulations, which treat unit operations like the contactor device as a black box. The construction of the flow sheet simulations utilizes mass and species conservation equations, chemical and thermodynamic data to fit experimental data to equilibrium equations (see, for example, references (5–7). The flow sheet simulations give the component concentration of every stage at steady-state as well as an estimate of the time to reach the steady-state. In addition, some fluid dynamical simulations have been performed for the two-fluid Taylor-Couette flow with an inner rotating cylinder and a stationary outer cylinder similar to the conditions of the mixing zone in a contactor (8, 9). Another study investigates the two-fluid Taylor-Couette flow in the gap between concentric, co-rotating cylinders (10).

In this paper, we simulate the separation of an aqueous and an organic stream in the rotor zone of one single contactor used in the actinide processing industry. We study the influence of the initial Organic to Aqueous (O/A) ratio inside the separation zone under the inflow of equal amounts of organic and aqueous materials. We show 2-dimensional (2D) simulations with the cylindrical symmetry of the separation zone. We, also, show 3-dimensional (3D) simulations of the same region. In these simulations, we have used the CartaBlanca (11) computer simulation program. This is a state-of-the-art multi-phase flow code environment, which uses advanced software design, and advanced nonlinear solver methods for the solution of multiphase flow equations on unstructured grids and complex geometries.

In addition to solvent extraction processes for metal-based solutes, the annular centrifugal contactor has been employed in other fields, as for example, the Pharmaceutical Industry (12) and in the Agricultural Food Products purification (13).

In what follows, we discuss the theoretical aspects of the calculations including the theoretical tools for the problem set up, the results and conclusions of our calculations.

THEORETICAL SECTION

Governing Equations

In this study, the isothermal flows require only mass and momentum conservation equations. The mass conservation equation for each phase, denoted by the index k, is:

$$\frac{\partial \theta_k \rho_k}{\partial t} + \nabla \cdot \theta_k \rho_k \vec{u}_k = 0, \tag{1}$$

where ρ_k is the constant mass density, $\vec{u}_k$ is the velocity, and θ_k is the volume fraction of the phase k satisfying the continuity condition, $\sum_k \theta_k = 1$. The momentum equation for each phase is given in the inertial frame by:

$$\frac{\partial \theta_k \rho_k \vec{u}_k}{\partial t} + \nabla \cdot (\theta_k \rho_k \vec{u}_k \vec{u}_k) = -\theta_k \nabla p + \sum_{l \neq k} F_{kl} + \theta_k \rho_k \vec{g} + \theta_k \nabla \cdot \tau_m \tag{2}$$

where p is the pressure, F_{kl} is the momentum exchange force between phase k and phase l, $\vec{g}$ is the gravity acceleration, and τ_m is the average viscous stress for the mixture. We model the stress as $\tau_m = 2\mu_{mixture}\, \mathrm{E}_{mixture}$, where $\mu_{mixture}$ is the effective viscosity of the mixture, and $\mathrm{E}_{\mathrm{mixture}}$ is the mixture strain rate calculated from the gradient of the mixture velocity $\vec{u}_m = \sum_k \theta_k \vec{u}_k$. The effective mixture viscosity can incorporate different physical effects and be a function not only the viscosities of the two phases and of the volume fraction, but also a function of the state of the flow. Given the lack of experimental data, we study numerically only the relative importance of the effective viscosity of the mixture by employing a simple model discussed in the Calculation Tools part of this section.

In this calculation, we consider only the momentum exchange due to drag:

$$F_{kl} = \theta_k \theta_l K_{kl} (\vec{u}_l - \vec{u}_k), \tag{3}$$

where K_{kl} is the momentum exchange coefficient. We model the momentum exchange coefficient using the model appropriate to a particulate or droplet phase dispersed throughout a continuous phase

$$K_{kl} = \frac{3}{4} \rho_{kl}^0 C_d \frac{|\vec{u}_l - \vec{u}_k|}{d_{kl}} \tag{4}$$

In equation (4), ρ_{kl}^0 is the material density of the continuous phase and C_d is the drag coefficient. The following relation between a spherical droplet with diameter d_{kl} and a Newtonian fluid was used

$$C_d = C_{d\infty} + \frac{24}{Re_{kl}} + \frac{6}{(1 + \sqrt{Re_{kl}})}, \tag{5}$$

with

$$Re_{kl} = \frac{|\vec{u}_k - \vec{u}_l| d_{kl}}{\nu_{kl}} \tag{6}$$

where ν_{kl} is the continuous phase kinematics viscosity. The expression in equation (5) is due to White (14). For this study, we had to estimate an effective droplet diameter since we did not have any direct observations of the droplets. We used a value of 0.015 cm based on a calibration which reproduces the measured (15) settling time from a simple experiment under the force of gravity.

A very important aspect of the liquid–liquid extraction is the mass transfer of a solute component from one of the phases to the other. We can describe the transfer of one component, in phase l with mass fraction χ_l to the phase k through the equations:

$$\begin{aligned} \frac{\partial \theta_l \rho_l \chi_l}{\partial t} + \nabla \cdot (\theta_l \rho_l \chi_l \vec{u}_l) &= \theta_l \theta_k K_{lk}^{MT} (\chi_l - \gamma \chi_k) \\ \frac{\partial \theta_k \rho_k \chi_k}{\partial t} + \nabla \cdot (\theta_k \rho_k \chi_k \vec{u}_k) &= -\theta_l \theta_k K_{lk}^{MT} (\chi_l - \gamma \chi_k) \end{aligned} \tag{7}$$

where the right hand side represents interphase mass transfer via a simple linear law. Here, K_{lk}^{MT} is the mass transfer coefficient and γ is the equilibrium distribution ratio. For demonstration purposes and for lack of better information on the mass transfer rates and equilibria, we use $K_{kl}^{MT} = 1.0$ and $\gamma = 0.1$ to calculate the mass transfer of one of the species in the aqueous phase l to the organic phase k. Once parameters are determined from further analyses, the method can be repeated with the appropriate values.

Calculations Tools

The Computational Meshes

In this study, we represent the separation zone of the contactor through 2D and 3D unstructured meshes. Figure 1 shows the three-dimensional mesh used in this calculation while Figure 2 shows both two-dimensional meshes used. The first one has vertical walls, the second one is inclined in relation to the vertical. The inclined-wall mesh was used to explore the effect of the geometry in the efficiency of the centrifugal contactors. Boycott (16) demonstrated, as long ago as 1920, that particles separated much faster from liquid by sedimentation if the container is tilted in relation to the direction of settling dictated by gravity. We have applied the same idea to the centrifugal contactors by designing the chamber with tilted sides.

The separation zone is 15.0 cm high. The internal radii are 0.3 cm and 0.8 cm above and below the diverter disc respectively. The diverter disc has

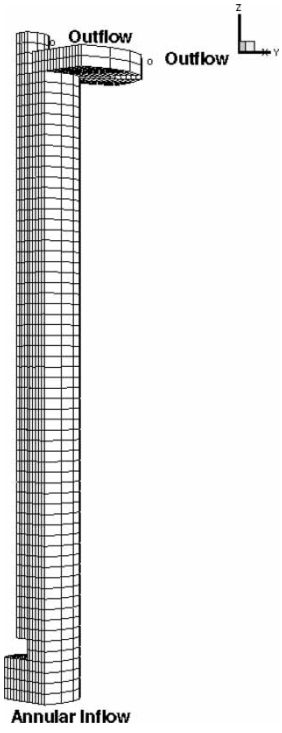

Figure 1. 3D mesh.

a 1.25 cm radius. We simplified the weirs at the top of the region considerably since we were interested only in the separation zone itself.

With the 2D meshes, we use the cylindrical symmetry capability of Carta-Blanca. In this case, the mixture flows into the region through an opening in the base. Considering the cylindrical symmetry, this represents an inflow through a ring. There are two outlets as indicated in the figure. In the upper inner outlet, we impose a pressure boundary condition. In the lower outer outlet, we impose a specified velocity boundary condition. Again, due to the cylindrical symmetry, these outlets represent the outflow through a circular region. The 3D mesh is a quarter section of the region.The liquids leave either through small holes, in a 3D mesh calculation or through circular outlets when using a 2D mesh and cylindrical symmetry. The meshes are unstructured.

Initial and Boundary Conditions

The inflow is a mixture of 50% aqueous and 50% organic phases. The aqueous phase, a solution of hydrochloric acid, has a density of $1.122\,\mathrm{gm/cm^3}$ and a viscosity of $0.0146\,\mathrm{dyne\text{-}s/cm^2}$, both unloaded. The organic phase, consisting

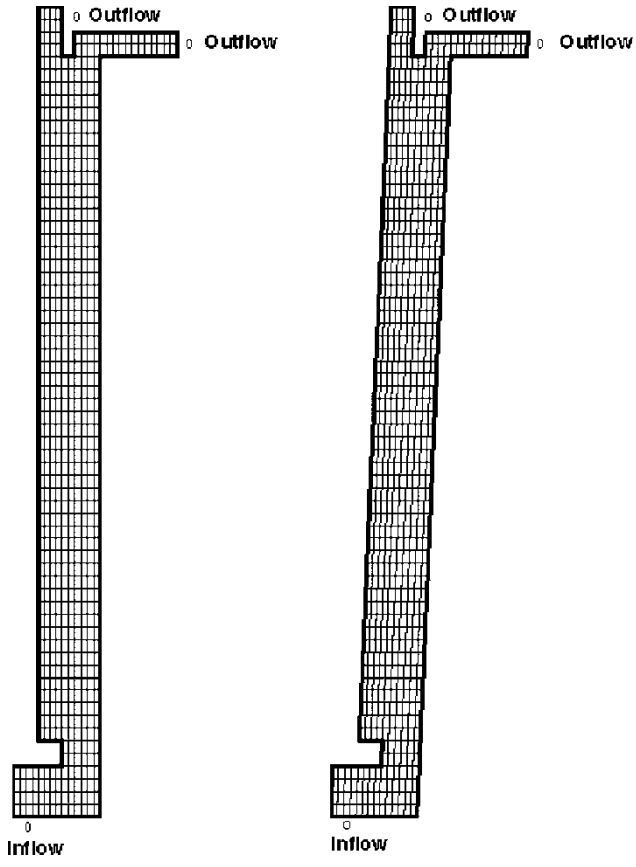

Figure 2. Straight and inclined 2D meshes.

of tri-butylphosphate in paraffinic hydro-carbon diluent, has a density of $0.7956\,\mathrm{gm/cm^3}$ and a viscosity of $0.1996\,\mathrm{dyne\text{-}s/cm^2}$, both unloaded. The mixture of liquids in the separation zone is initially at rest. We varied the volume fractions of the phases. We used, in different calculations, for the aqueous phase volume fractions of 1.0, 0.75, 0.5, and 0.0. The inflow velocity is specified to give throughput of $500\,\mathrm{mL/s}$. The specified velocity at the outflow is calculated supposing that half of the mixture leaves the device through the outer outlet.

Effective Viscosity

A rigorous description of the effective mixture viscosity constitutes an extremely complex field and is out of the scope of the present paper. We approach approximating the mixture viscosity using Einstein's (17)

pioneering derivation of an expression for viscosity of a dilute suspension of solid spheres. Since his work, considerable effort, both theoretical and empirical, has been dedicated to extending the theory to higher concentrations of particles (see, for example, references 18–26). In a two-phase flow of immiscible fluids, the liquid with considerably higher volume fraction, usually, constitutes the continuous phase, and the one with lower volume fraction constitutes the dispersed phase. At a particular volume fraction, we may have a phase inversion point in which the continuous phase becomes dispersed and vice-versa. For a certain range of volume fractions, the ambivalent range, either phase can be the continuous one. Phase inversion has also been studied extensively (see references 27–31 as an example).

To estimate the effective viscosity of this system, we use an exponential form for computing the effective viscosity, as proposed by Chen and Law (26):

$$\mu_r = \exp\left[\frac{2.5}{\beta}\left(\frac{1}{(1-\theta_d)^{\beta}} - 1\right)\right] \tag{8}$$

In the formula above, $\mu_r = \mu_{eff}/\mu_c$, with μ_c the viscosity of the pure continuous phase and μ_{eff} is the effective viscosity of the continuous phase. θ_d is the volume fraction of the dispersed phase. The exponent β can be varied to represent different empirical relationships. For example, the value of $\beta = 2$, in equation (8) reproduces the values reported by Frankel and Acrivos (23). The value of 0.95 reproduces the high shear values of Barnes et al. (24).

In our simulation, we tried both the values of 2 and 0.95 for the exponent β. We made the assumption that each phase could be dispersed if its volume fraction varied from 0.0 to 0.6. In the region of volume fractions from 0.0 to 0.4, we use expression (8) for the effective viscosity of the continuous phase. If the volume fractions were 0.4 to 0.6, we used the effective viscosity value obtained for the volume fraction equal to 0.4. This choice, although arbitrary, is suitable for our estimation purposes.

Figure 3 shows the values of the relative viscosity μ_r when each phase is the continuous for both β equals 2 and 0.95. For each value of β we have two curves: The red curve is for continuous aqueous phase and the green one is for continuous organic phase.

For estimating the effective viscosity of the mixture, we use the expression below which is plotted in Fig. 4:

$$\mu_{mixture} = \theta_{aqueous}\mu_{eff}^{aqueous} + \theta_{organic}\mu_{eff}^{organic} \tag{9}$$

where μ_{eff} for each phase (aqueous or organic) is set to zero if the volume fraction of this phase is smaller than 0.4. Using this approach,the mixture effective viscosity approaches the correct limits for both pure organic or

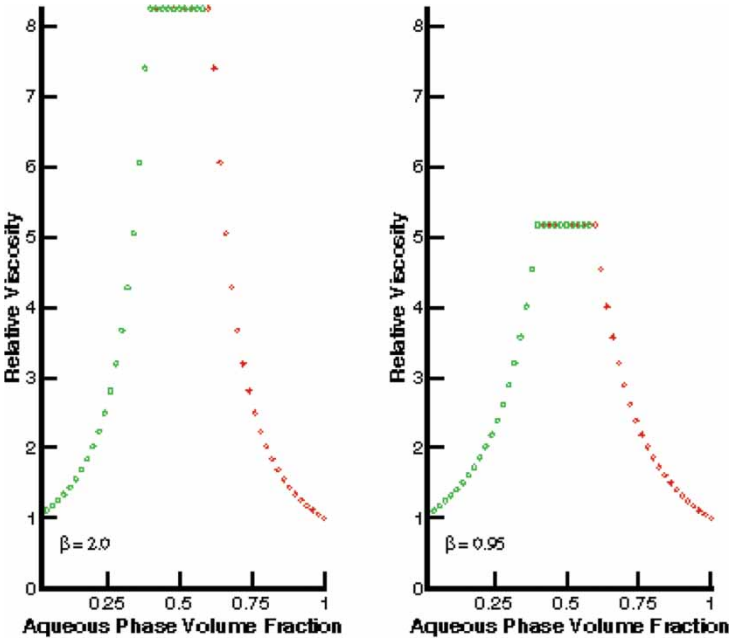

Figure 3. Relative viscosity: red symbols for continuous aqueous phase; green symbols for continuous organic phase.

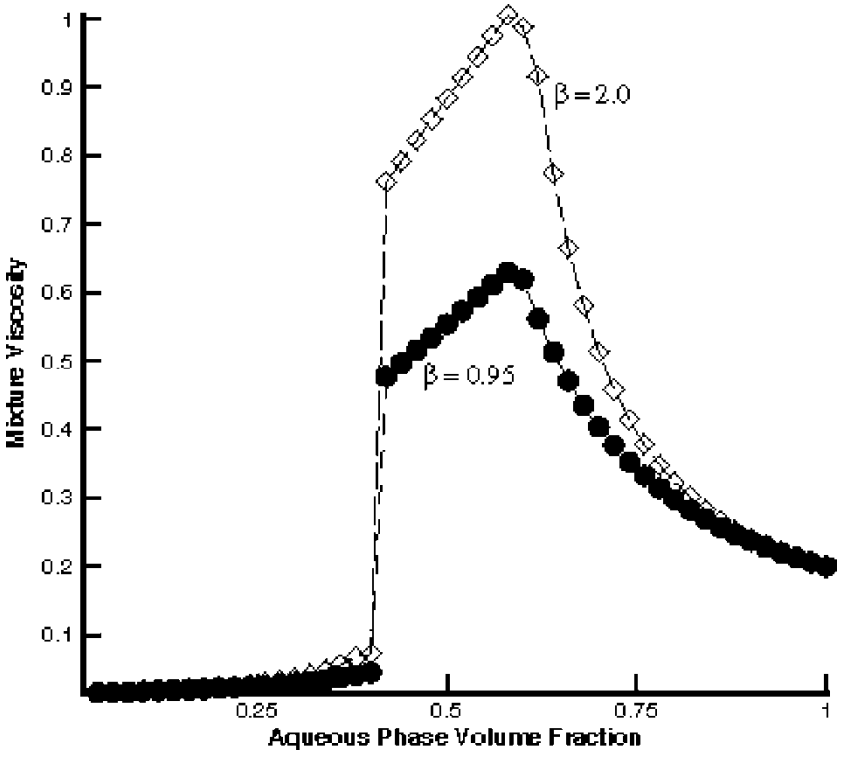

Figure 4. Viscosity of the mixture in dynes-s/cm^2.

pure aqueous fluids. It also predicts very high values for the viscosity of the mixture when the volume fraction of the continuous organic phase decreases, as observed by Leonard (2).

Figure 4 shows a strong asymmetry in the mixture viscosity curve. The viscosity for the continuous organic phase (low volume-fraction aqueous-phase) is quite small and rises suddenly. The viscosity for the continuous aqueous phase (high aqueous-phase volume-fraction) is much higher, not climbing as rapidly.

We also considered a simpler expression for the viscosity of the mixture:

$$\mu_{mixture} = \theta_{aqueous}\mu_{aqueous} + \theta_{organic}\mu_{organic} \tag{10}$$

with $\mu_{aqueous}$ the viscosity of the pure aqueous phase and $\mu_{organic}$ the viscosity of the pure organic phase. This was motivated by the fact that for intermediate mixture ratios, the particle-fluid morphology is probably not a reasonable representation of the microstructure.

RESULTS AND DISCUSSION

Single Stage Hydraulic Process

Figures 5 and 6 show the 2D cylindrical symmetry results for single-stage hydraulic performance, at steady-state, when the separation zone was, initially, filled with a mixture containing 50% aqueous phase and rotated at 1000 rpm and 3000 rpm, respectively. The first figure of each series (A) was calculated with the viscosity of expression 10; the second figure (B) used the viscosity of expression 9, with $\beta = 2.0$, and the third one (C) also used the viscosity of expression 9 but with $\beta = 0.95$.

A comparison of Figs. 5 and 6 illustrates how the higher angular velocity overcomes the effect of the gravity.

Figures 7 and 8 bring similar results but with the initial volume fraction of 0.75 for the aqueous phase.

The different results above for the cases with differing initial aqueous volume fraction illustrate how the initial composition may influence the contamination at each phase outlet by the opposite phase material. This may suggest the possibility of multiple steady states, at least in the simulations. Also, different viscosities seem to be more important in the cases with initial aqueous volume fraction 0.75 than in the cases where this value is 0.5. The effect is more pronounced in the lower angular velocity case, as it should be expected.

We repeated the simulations above using the tilted mesh. This allowed us to see the advantages of having a different device with the inclined walls using gravity to help the separation. Figures 9 through 12 show the densities of the aqueous phase in the inclined device.

Figure 13 shows the 3D results for the aqueous phase density at 1000 rpm when, initially the device contained a 75% aqueous phase in the mixture. For the case of the inclined geometry, in contrast to the vertical geometry, we see no evidence of multiple steady states in the solutions.

Mass Transfer

Figures 14 and 15 show the mass fraction of the species transferred from the aqueous phase to the organic phase for both the straight and inclined meshes. Initially, the mixture consists of 50% aqueous phase and 50% organic phase with two species in each phase. The aqueous phase has 5% of a heavy material, with density $19.98\,\mathrm{g/cm^3}$ and 95% of the same aqueous material used in the hydraulics-only simulations. The organic phase consists of 0% of the heavy material and 100% of the same organic phase considered in the hydraulic simulations. After reaching steady state, some of the heavy material is transferred from the aqueous phase to the organic phase. Figure 14 shows the results for the contactor at 3000 rpm and Figure 15 at 1000 rpm.

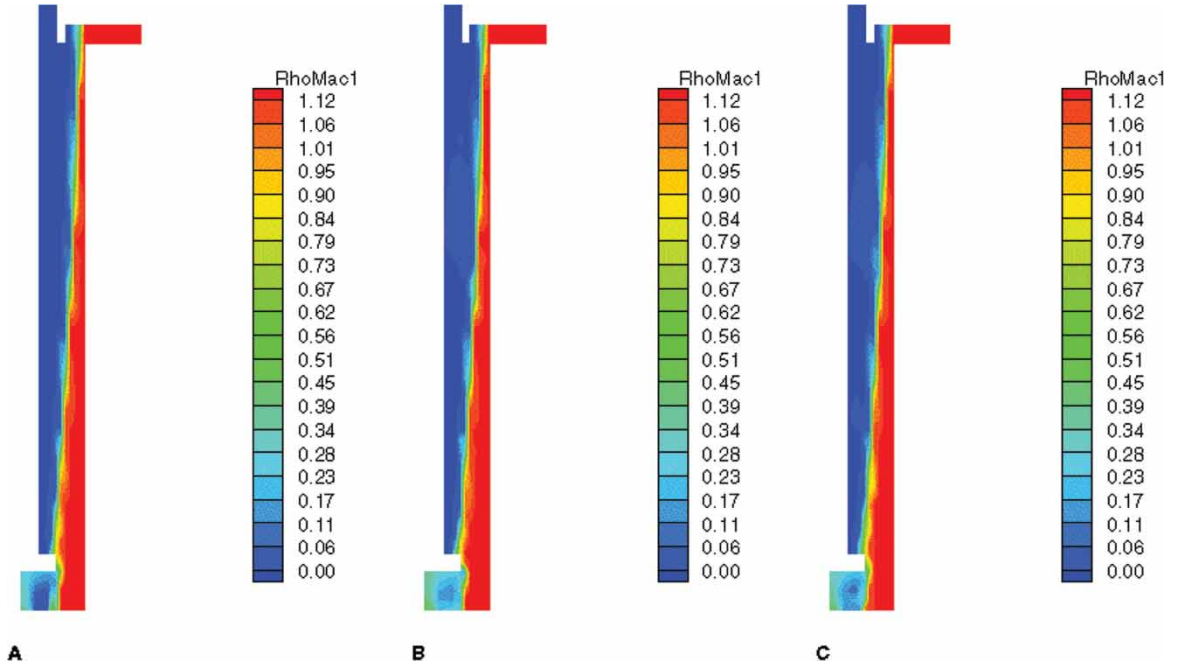

Figure 5. Aqueous-phase density at 1000 rpm and, initially, 0.5 aqueous-phase volume-fraction.

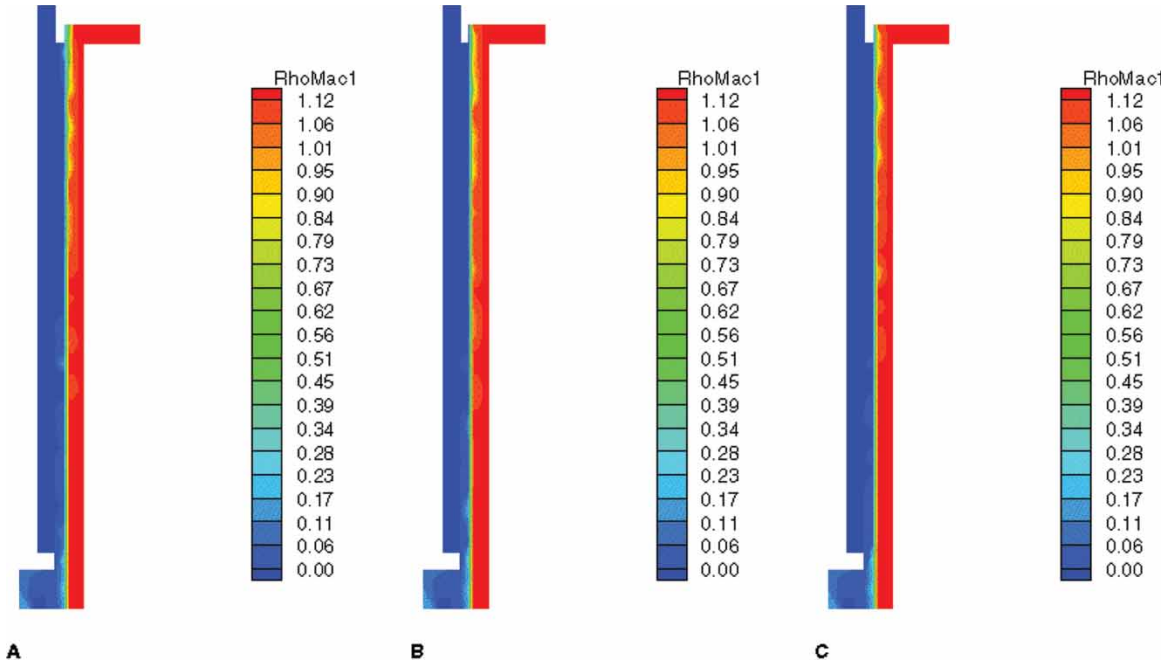

Figure 6. Aqueous-phase density at 3000 rpm and, initially, 0.5 aqueous-phase volume-fraction.

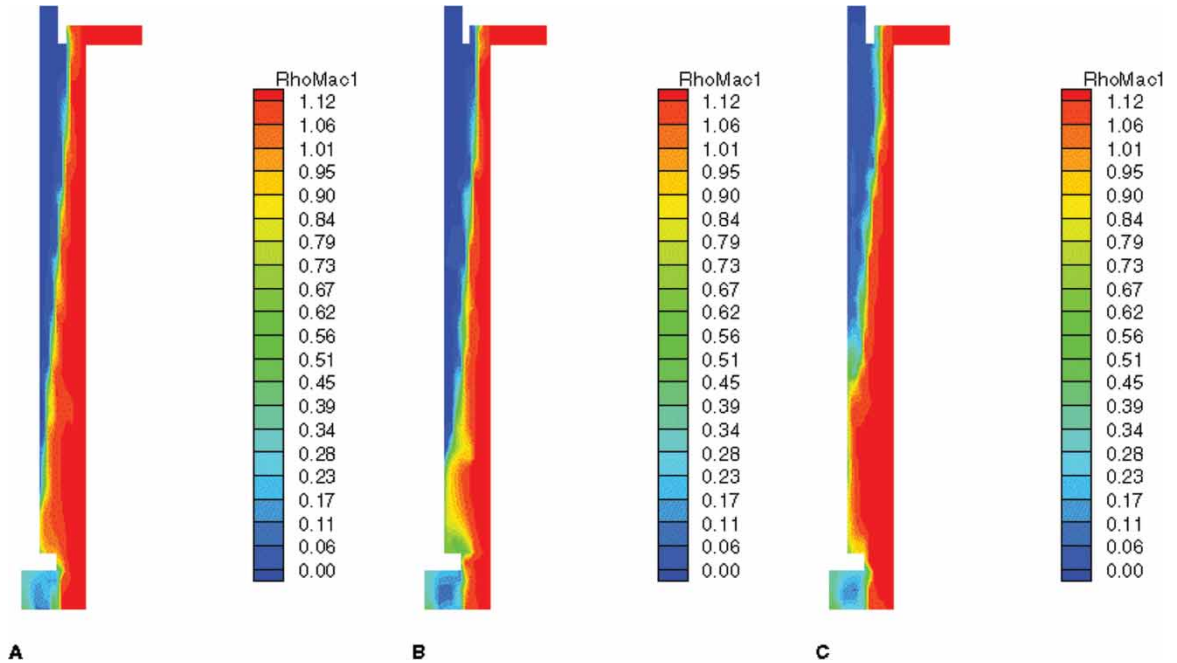

Figure 7. Aqueous-phase density at 1000 rpm and, initially, 0.75 aqueous-phase volume-fraction.

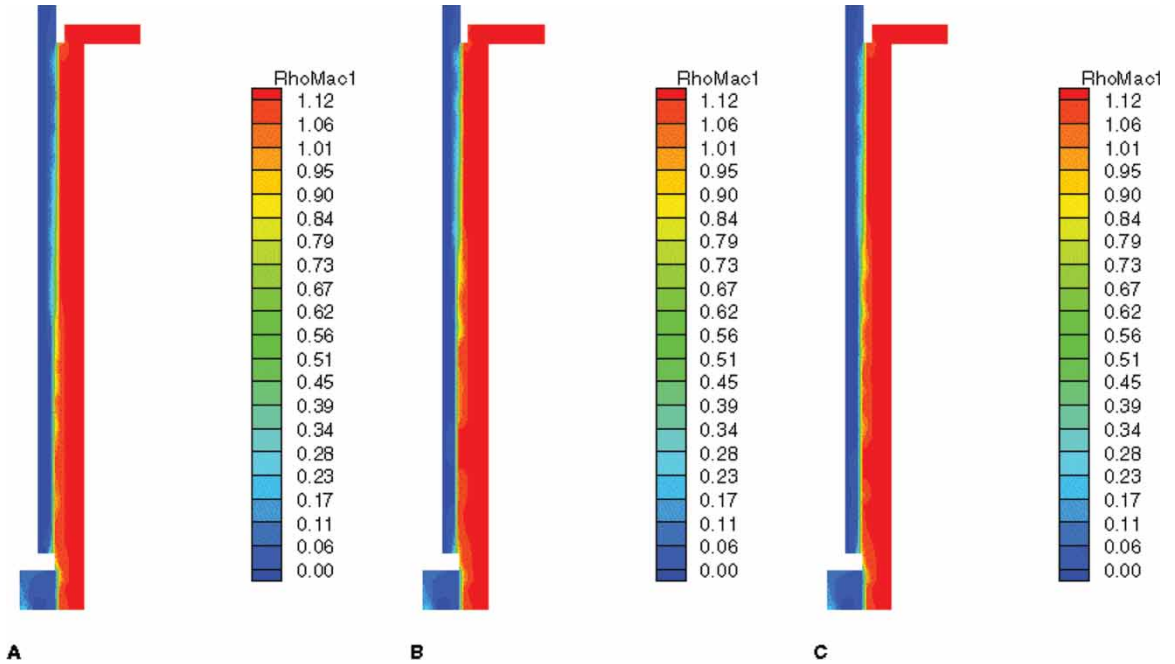

Figure 8. Aqueous phase density at 3000 rpm and, initially, 0.75 aqueous-phase volume-fraction.

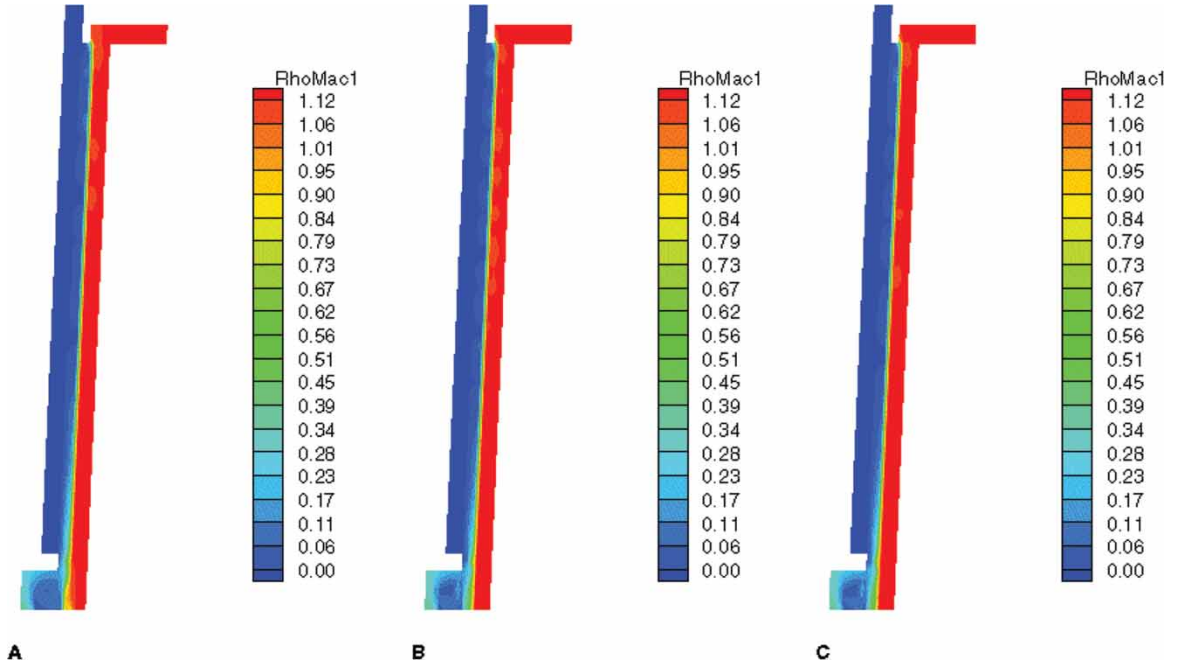

Figure 9. Aqueous phase density at 1000 rpm and, initially, 0.5 aqueous-phase volume-fraction.

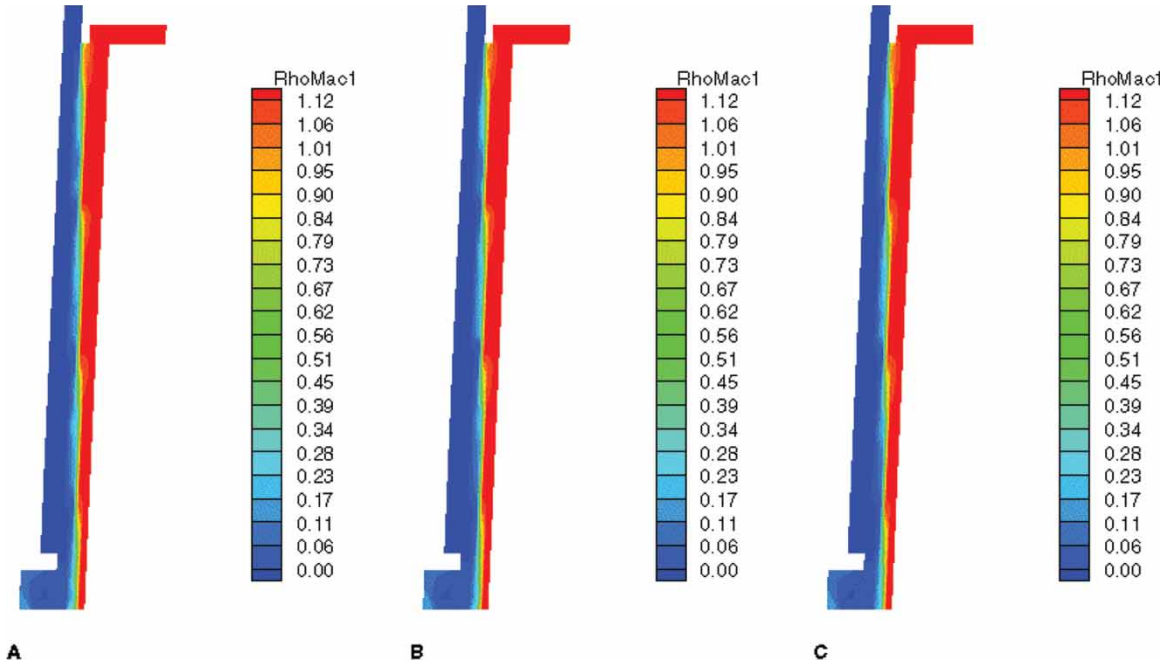

Figure 10. Aqueous-phase density at 3000 rpm and, initially, 0.5 aqueous-phase volume-fraction.

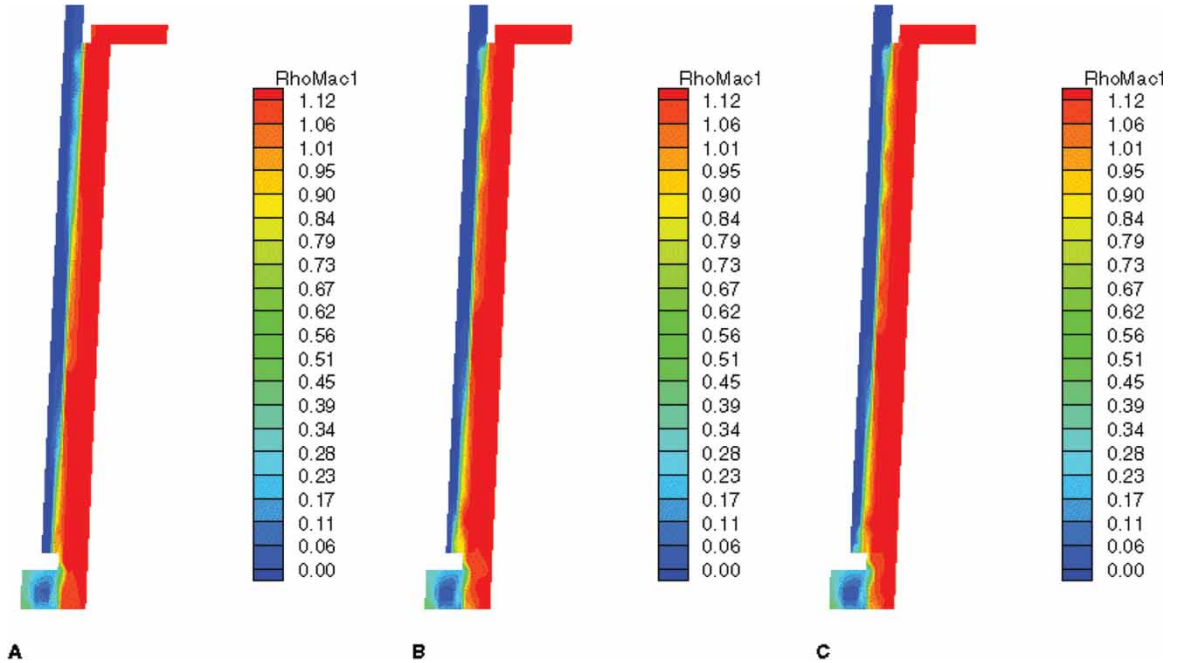

Figure 11. Aqueous phase density at 1000 rpm and, initially, 0.75 aqueous-phase volume-fraction.

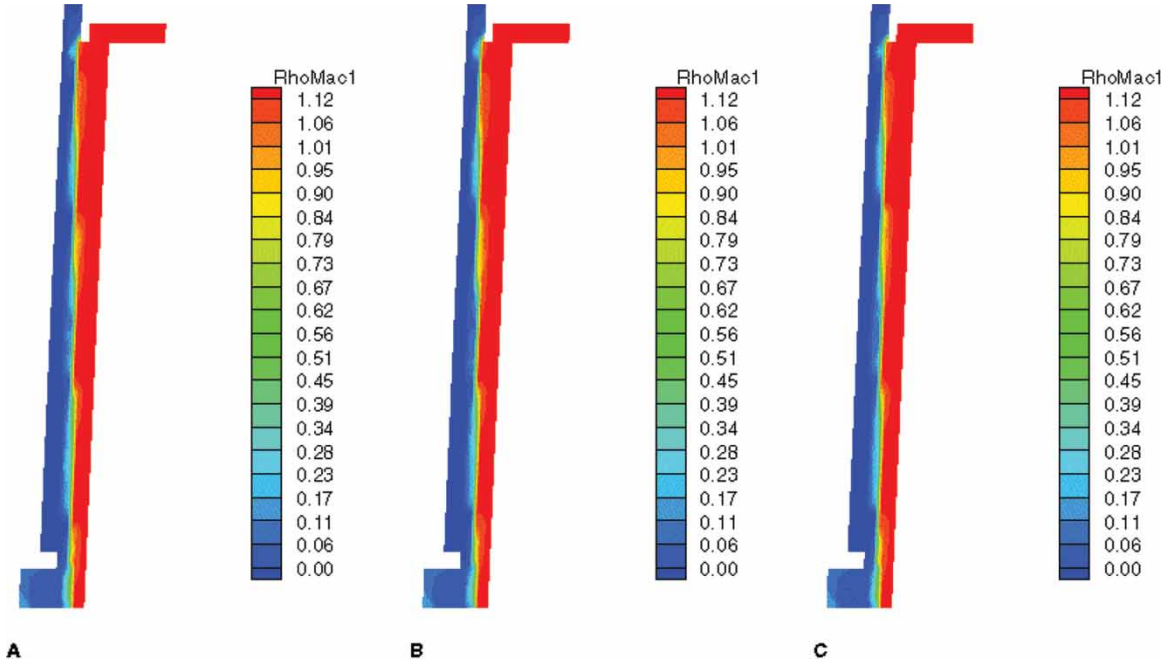

Figure 12. Aqueous phase density at 3000 rpm and, initially, 0.75 aqueous phase volume fraction.

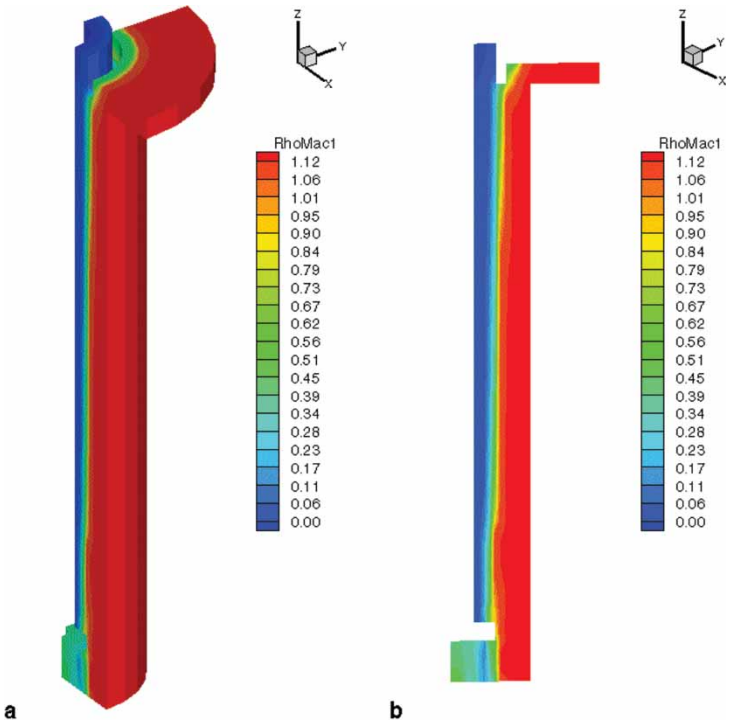

Figure 13. 3D results for the aqueous phase density after an initial mixture with 75% aqueous phase: a) 3D display; b) Cut at 45° of the results shown in (a).

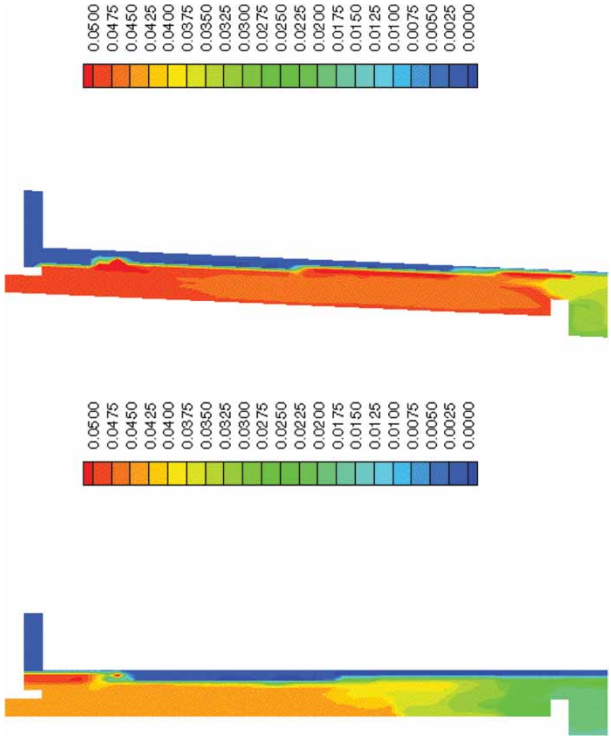

Figure 14. Steady-state heavy-species mass-fraction in the aqueous-phase at 3000 rpm.

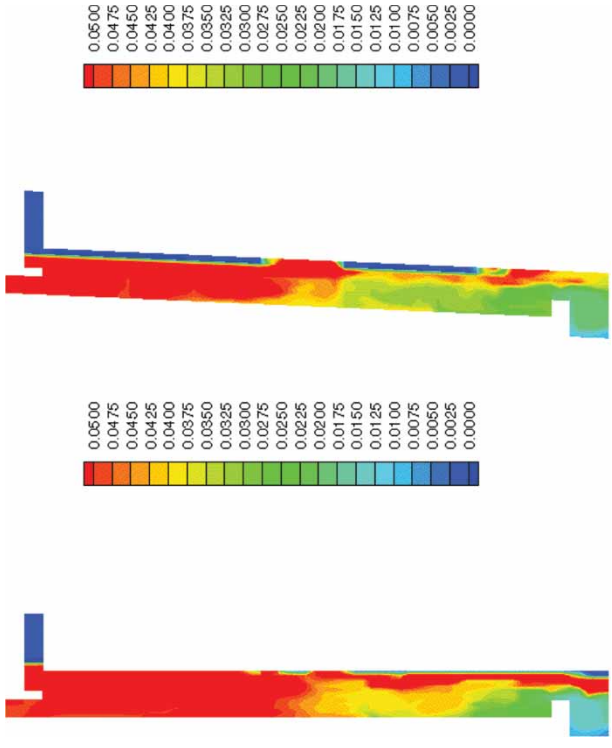

Figure 15. Steady-state heavy-species mass-fraction in the aqueous-phase at 1000 rpm.

For the rotation zone at 3000 rpm, we see much better mass transfer for the inclined device. This does not seem to be the case for the zone at 1000 rpm as we see in Figure 15.

CONCLUSIONS

We have solved the momentum and mass conservation equations in the simulation of the separation of the aqueous and the organic components in the rotor zone of a centrifugal contactor. We have demonstrated a computational scheme and a tool which can be used to examine complex hydraulics, to explore effects of the geometry in the process, and to study the influence of different initial conditions, distinct rotor speeds, and diverse physical contributions. We have studied the importance of the effective viscosity. Its effect seems important at the low and high angular velocities, especially, for the vertical contactor case. Since the objective is to reach very high extraction-efficiency, the more accuracy in the modeling of effective viscosity in the simulations may be necessary. The calculations also show a potentially strong effect from mass transfer on the dynamics, indicating the need for realistic mass transfer parameters before more definitive statements can be made.

Ultimately, these simulations aim at improving the efficiency of the centrifugal contactors by allowing, for example, investigation of alternative shapes for the devices or suggesting more appropriate initial conditions. Both of these had significant effects in our simulations. Future plans include the evaluation and optimization of advanced designs for contactors as well the investigation of the issue of scale to determine the minimum size for pilot units.

REFERENCES

1. Berstein, G.J., Grosvenor, D.E., Lenc, J.F., and Levitz, N.M. (1973) A high-capacity annular centrifugal contactor. *Nucl. Tech.*, 20: 200–202.
2. Leonard, R.A., Bernstein, G.J., Ziegler, A.A., and Pelto, R.H. (1980) Annular centrifugal contactors for solvent extraction. *Sep. Sci. Technol.*, 15: 925–943.
3. Leonard, R.A., Pelto, R.H., Zeigler, A.A., and Bernstein, G.J. (1980) Flow over circular wires in a centrifugal field. *Can. J. Chemical Eng.*, 58 (4): 531–534.
4. Leonard, R.A. (1988) Recent advances in centrifugal contactor design. *Sep. Sci. Technol.*, 23: 1473–1487.
5. Leonard, R.A. (1987) Use of electronic worksheets for calculation of stagewise solvent extraction processes. *Sep. Sci. Technol.*, 22 (2&3): 535–556.
6. Leonard, R.A. and Regalbuto, M.C. (1994) Spreadsheet algorithm for stagewise solvent extraction. *Solvent Extraction and Ion Exchange*, 12 (5): 909–930.
7. Wallwork, A.L., Denniss, I.S., Taylor, R.J., Bothwell, P., Birkett, J.E., and Baker, S. (1999) Modelling of advanced flow sheets using data from miniature contactor trials. *Nuclear Energy*, 38 (1): 31–35.
8. Leonard, R.A., Bernstein, G.J., Pelto, R.H., and Zeigler, A.A. (1981) Liquid–liquid dispersion in turbulent Couette flow. *AIChE Journal*, 27 (3): 495–503.

9. Renardy, Y. and Joseph, D.D. (1985) Couette flow of two fluids between concentric cylinders. *J. Fluid Mech.*, 150: 381–394.
10. Baier, G. and Graham, M.D. (1998) Two-fluid Taylor-Couette flow: Experiments and linear theory for immiscible liquids between corotating cylinders. *Phys. Fluids*, 10 (12): 3045–3053.
11. VanderHeyden, W.B., Dendy, E.D., and Padial-Collins, N.T. (2002) CartaBlanca-A pure-Java, component-based systems simulation tool for coupled nonlinear physics on unstructured grids–an update. *Concurrency and Computat: Pract. Exper.*, 14: 1–28.
12. Meikrantz, D.H., Macaluso, L.L., Heald, C.J., Mendoza, G., and Meikrantz, S.B. (2002) A new annular centrifugal contactor for pharmaceutical process. *Chem. Eng. Comm.*, 189 (12): 1629–1639.
13. See, for example, specifications for Agricultural Products Centrifugal Contactors in http://www.rousselet-robatel.com/products/lx.php.
14. White, F.M. (1974) *Viscous Fluid Flow*; McGraw Hill: NY.
15. Yarbro, S.L. and Schreiber, S.B. (2003) Using process intensification in the actinide processing industry. *J. Chem. Technol. Biotechnol.*, 78: 254–259.
16. Boycott, A.E. (1920) Sedimentation of blood corpuscles. *Nature*, 104: 532.
17. (a) Einstein, A. (1906) A new determination of molecular dimensions. *Ann. Phys.*, 19: 289–306; (b) Einstein, A. (1911) The theory of the Brownian movement. *Ann. Phys.*, 1911, 34: 591–592.
18. Arrhenius, S. (1917) The viscosity of solutions. *Biochem. J.*, 11: 112–133.
19. Eilers, H. (1941) Die Viskositat von Emulsionen hochviskoser Stoffe als Funktion der Konzentration. *Kolloid Z.*, 97: 313–321.
20. Mooney, M. (1951) The viscosity of a concentrated suspension of spherical particles. *J. Colloid. Sci.*, 6: 162–170.
21. Rutgers, I.R. (1962) Relative viscosity and concentration. *Rheol. Acta*, 2: 305–348.
22. Thomas, D.G. (1965) Transport characteristics of suspensions. *J. Colloid. Sci.*, 20: 267–277.
23. Frankel, N.A. and Acrivos, A. (1967) On the viscosity of concentrated suspension of solid spheres. *Chem. Eng. Sci.*, 22: 847–853.
24. Barnes, H.A., Hutton, J.F., and Walters, K. (1989) *An Introduction to Rheology*; Elsevier: Amsterdam, The Netherlands.
25. Cheng, N.S. and Law, W.K.A. (2003) Exponential formula for computing effective viscosity. *Powder Technology*, 129: 156–160.
26. Hsueh, C.-H. and Becher, P.F. (2005) Effective viscosity of suspensions of spheres. *J. Am. Ceram. Soc.*, 88 (4): 1046–1049.
27. Selker, A., Sleicher, C.A., Jr. (1965) Factors affecting which phase will disperse when immiscible liquids are stirred together. *Can. J. Chem. Eng.*, 43 (6): 298–301.
28. Nadler, M., Mewes, D. (1997) Flow induced emulsification in the flow of two immiscible liquids in horizontal pipes. *Int. J. Multiphase Flow*, 23 (1): 55–68.
29. Brauner, N. and Ullmann, A. (2002) Modeling of phase inversion phenomenon in two-phase pipe flows. *Int. J. Multiphase Flow*, 28: 1177–1204.
30. Lhuillier, D. (2003) Dynamics of interfaces and rheology of immiscible liquid–liquid mixtures. *C. R. Mecanique*, 331: 113–118.
31. Ioannou, K. and Jorgen, Nydal O.Angeli, P. (2005) Phase inversion in dispersed liquid–liquid flows. *Exp. Therm. Fluid Sci.*, 29: 331–339.